SCIENCE CHINA Materials ARTICLES

mater.scichina.com link.springer.com

Published online 27 March 2020 | https://doi.org/10.1007/s40843-020-1274-0
Sci China Mater 2020, 63(7): 1163–1170

Novel layered $K_{0.7}Mn_{0.7}Ni_{0.3}O_2$ cathode material with enlarged diffusion channels for high energy density sodium-ion batteries

Jinghui Chen, Zhitong Xiao, Jiashen Meng, Jinzhi Sheng, Yanan Xu, Junjun Wang, Chunhua Han and Liqiang Mai*

ABSTRACT **As promising, low-cost alternatives of lithium-ion batteries for large-scale electric energy storage, sodium-ion batteries (SIBs) have been studied by many researchers. However, the relatively large size of Na^+ leads to sluggish diffusion kinetics and poor cycling stability in most cathode materials, restricting their further applications. In this work, we demonstrated a novel K^+-intercalated Mn/Ni-based layered oxide material ($K_{0.7}Mn_{0.7}Ni_{0.3}O_2$, denoted as KMNO) with stabilized and enlarged diffusion channels for high energy density SIBs. A spontaneous ion exchange behavior in forming $K_{0.1}Na_{0.7}Mn_{0.7}Ni_{0.3}O_2$ between the KMNO electrode and the sodium ion electrolyte was clearly revealed by *in situ* X-ray diffraction and *ex situ* inductively coupled plasma analysis. The interlayer space varied from 6.90 to 5.76 Å, larger than that of $Na_{0.7}Mn_{0.7}Ni_{0.3}O_2$ (5.63 Å). The enlarged ionic diffusion channels can effectively increase the ionic diffusion coefficient and simultaneously provide more K^+ storage sites in the product framework. As a proof-of-concept application, the SIBs with the as-prepared KMNO as a cathode display a high reversible discharge capacity (161.8 mA h g^{-1} at 0.1 A g^{-1}), high energy density (459 W h kg^{-1}) and superior rate capability of 71.1 mA h g^{-1} at 5 A g^{-1}. Our work demonstrates that the K^+ pre-intercalation strategy endows the layered metal oxides with excellent sodium storage performance, which provides new directions for the design of cathode materials for various batteries.**

Keywords: $K_{0.7}Mn_{0.7}Ni_{0.3}O_2$, K^+ pre-intercalation, enlarged layered structure, high energy density, sodium-ion batteries

INTRODUCTION

Nowadays, with the rapid development of consumer electronics, portable devices and electric vehicles, rechargeable power sources with high energy densities and low costs are highly desired [1–3]. The further development of rechargeable lithium-ion batteries (LIBs) in practical applications is hindered by the high cost and scarcity of lithium resource [4–6]. Recently, sodium-ion batteries (SIBs) have been widely investigated as a new kind of energy storage system due to the similar working principle with LIBs, safety and low cost [7–17]. Cathode materials with an excellent operating voltage and high specific capacity are crucial for the successful development of high energy density SIBs [18–22]. Among most cathode materials for SIBs [23–29], P2-type Mn/Ni-based binary metal oxide material is considered as one of the most promising candidates due to its high operating potential ($Ni^{2+/4+}$ redox reaction), but its practical application is impeded by the low specific capacity and poor cycling stability [20–32].

Certainly much effort is put in to enhance the electrochemical property of Mn/Ni-based oxide cathode materials. One efficient strategy is doping divalent ions to supersede nickel ion, which can restrain the undesired phase transition and maintain the structure stability [33–35]. Wang *et al.* [33] demonstrated Mg-doped $Na_{0.67}Mn_{0.67}Ni_{0.28}Mg_{0.05}O_2$ with a reversible capacity of 123 mA h g^{-1}, and a capacity retention of approximately 85% after 50 cycles. Another efficient approach is surface modification by coating a shell to provide protection, and then increase the cycle stability. Liu *et al.* [36] designed a Al_2O_3-coated $Na_{2/3}Mn_{2/3}Ni_{1/3}O_2$, which exhibited a reversible capacity of 115 mA h g^{-1} after 300 cycles. Most of these methods reported by previous work increase the

State Key Laboratory of Advanced Technology for Materials Synthesis and Processing, International School of Materials Science and Engineering, Wuhan University of Technology, Wuhan 430070, China
* Corresponding author (email: mlq518@whut.edu.cn)

cycle stability of such P2-type Mn/Ni-based layered oxides, while the problem of low reversible capacity is neglected. Therefore, the improvement of reversible capacity in this type layered oxide is desired [37–40]. In previous studies, a fascinating K^+ pre-intercalation approach was exploited, which enlarged the interlayer spacing to expand the diffusion channels, and then improved the cycling stability and rate capability of the electrode materials [41,42]. The pre-intercalation strategy is supposed to be an effective way to enlarge ionic diffusion channels, stabilize interlayer structures, and improve the electrochemical performance of such layered oxides.

In this work, we designed and constructed a K^+ pre-intercalated Mn/Ni-based layered oxide ($K_{0.7}Mn_{0.7}Ni_{0.3}O_2$, denoted as KMNO) by a facile solid phase sintering method, and investigated the effect of KMNO on the sodium storage performances. As a cathode material in SIBs, the obtained KMNO shows a high reversible discharge capacity of 161.8 mA h g^{-1} at 0.1 A g^{-1}, satisfactory cycling performance with a 82.3% capacity retention after 500 cycles at 0.5 A g^{-1} and a high rate property of 71.1 mA h g^{-1} at 5 A g^{-1}. The Na^+ intercalation/deintercalation mechanism of KMNO electrode was studied by *ex situ* transmission electron microscopy (TEM) mapping and *ex situ* X-ray diffraction (XRD). The diffusion kinetics of KMNO was analyzed *via* the galvanostatic intermittent titration technique (GITT) measurement. In addition, our work proposes that K^+ pre-intercalation is a facile and effective approach to enhance the electrochemical property of layered oxide cathode materials for SIBs.

EXPERIMENTAL SECTION

Synthesis of KMNO and $Na_{0.7}Mn_{0.7}Ni_{0.3}O_2$ (NMNO)

The KMNO and NMNO particles were synthesized by solid phase reactions. First, 4 g of polyvinylpyrrolidone (PVP, average M_w = 4000) was dissolved in 40 mL of deionized water, which was magnetic stirred vigorously for 1 h at room temperature. Second, 3.675 mmol of potassium acetate (CH_3COOK, 99%, 5% potassium source excess), 3.5 mmol of manganese (II) acetate tetrahydrate ($Mn(CH_3COO)_2{\cdot}4H_2O$, 99%) and 1.5 mmol of nickel (II) acetate tetrahydrate ($Ni(CH_3COO)_2{\cdot}4H_2O$, 99%) were dissolved in PVP solution (PVP acted as a dispersant, which made the solution viscous and uniform) with vigorous stirring at room temperature for another 10 h. Then, the mixture was dried in an oven at 70°C for 12 h. The solid from the previous steps was firstly pre-sintered in muffle furnace at 300°C for 2 h and then sintered in air at 900°C for 10 h. The heating rate of the muffle furnace was 5°C min^{-1}. As a comparison, the NMNO was synthesized using the same processes, with sodium acetate trihydrate ($CH_3COONa{\cdot}3H_2O$, 99%) used as the alkali-metal-ion sources. All synthetic materials were transferred directly to an argon filled glovebox (MBraun, O_2 and $H_2O \leq 0.01$ ppm).

Structural characterizations

The XRD patterns to investigate the crystallographic structure were performed by using a D8 Discover X-ray diffractometer, with Cu Kα radiation (λ = 1.5418 Å). Scanning electron microscopy (SEM) images were obtained using a JEOL JSM-7100F SEM/EDS microscope at an acceleration voltage of 20 kV. TEM, high resolution TEM (HRTEM) and selected area electron diffraction (SAED) images were collected by a JEM-2100F/Titan G2 60-300 transmission electron microscope. Energy dispersive spectroscopy (EDS) mapping was performed using an EDXGENESIS 60S spectrometer. Inductively coupled plasma (ICP) tests were performed using a PerkinElmer Optima 4300DV spectrometer.

Electrochemical measurement

The electrochemical properties were characterized by assembling 2016 coin cells in a glove box ($O_2 \leq 0.01$ ppm and $H_2O \leq 0.01$ ppm), with Na metal (99.5%, Sigma-Aldrich) as the reference electrode. 1 mol L^{-1} $NaClO_4$ in a mixture of ethylene carbon (EC) and propylene carbonate (PC) (*v*:*v* = 1:1) and 5.0 wt% fluoroethylene carbonate (FEC) (electrolyte additive) were used as the electrolyte, and a Whatman glass fiber (grade GF/D) was used as the separator. To obtain the cathode materials, 70 wt% as-synthesized active materials, 20 wt% acetylene black and 10 wt% polyvinylidene fluoride (PVDF) were mixed in *N*-methyl-2-pyrrolidone (NMP). The loading of the active material was approximately 1.6–1.8 mg cm^{-2}. The aluminum foil coated with active materials was dried at 70°C in a vacuum oven overnight. Galvanostatic charge/discharge tests were performed over the potential range from 2.0 to 4.0 V *vs.* Na^+/Na by using a multichannel battery testing system (LAND CT2001A). Cyclic voltammetry (CV) and electrochemical impedance spectroscopy (EIS) were conducted by using an electrochemical workstation under the alternating current ranging from 0.01 Hz to 10 kHz (CHI600E and Autolab PGSTAT 302N). GITT was used at each 5-min step of charge/discharge with a current flux of 10 mA g^{-1} followed by a 1 h relaxation step. The diffusion coefficient of Na^+ was measured by using GITT and calculated based on the

following equation:

$$D = \frac{4L^2}{\pi\tau}\left(\frac{\Delta E_s}{\Delta E_t}\right)^2,$$

where t and τ represent the duration of current pulse (s) and relaxation time (s), respectively. L corresponds to the Na^+ diffusion length, which is equal to the thickness of electrode. ΔE_s and ΔE_t are the steady-state voltage change (V) by the current pulse and voltage change (V) during the constant current pulse (eliminating the voltage changes after relaxation time)

RESULTS AND DISCUSSION

The XRD patterns of KMNO and NMNO obtained by a simple solid-phase reaction show obvious crystalline phases (Fig. 1a). The XRD pattern of KMNO is similar to that of NMNO, suggesting a similar layered structure. In particular, the d-spacing of the KMNO is 6.90 Å (2θ = 12.81°), ~1.22 times higher than that of NMNO (5.63 Å), verifying the expanded interlayer spacing. Furthermore, the results of the ICP measurement show that the K:Mn:Ni and Na:Mn:Ni molar ratios of the as-prepared KMNO and NMNO are 0.700:0.706:0.298 and 0.700:0.708:0.305, respectively (Table S1), corresponding to the expected stoichiometry. From the SEM and TEM images, two samples have similar particle morphologies with a size range of 0.5–2 μm (Fig. 1b–d and g). HRTEM images clearly display the measured interlayer distances of KMNO and NMNO are ~0.244 and ~0.229 nm, respectively, which are in agreement with the (102) plane of the layered structure (Fig. 1e, h). The single-crystalline hexagonal structures of the two samples are demonstrated by their SAED patterns (inset of Fig. 1e, h). High angle annular dark-field scanning-TEM (HAADF-STEM) images further confirm the K, Mn, Ni elements are uniformly distributed on KMNO and Na, Mn, Ni elements on NMNO, respectively (Fig. 1f, i).

The superior performances of KMNO as an SIB cathode material compared with NMNO are demonstrated by electrochemical characterizations (Fig. 2). The multiple cathodic/anodic peaks are observed in CV curves (Fig. 2a). The first four sodiation/disodiation processes

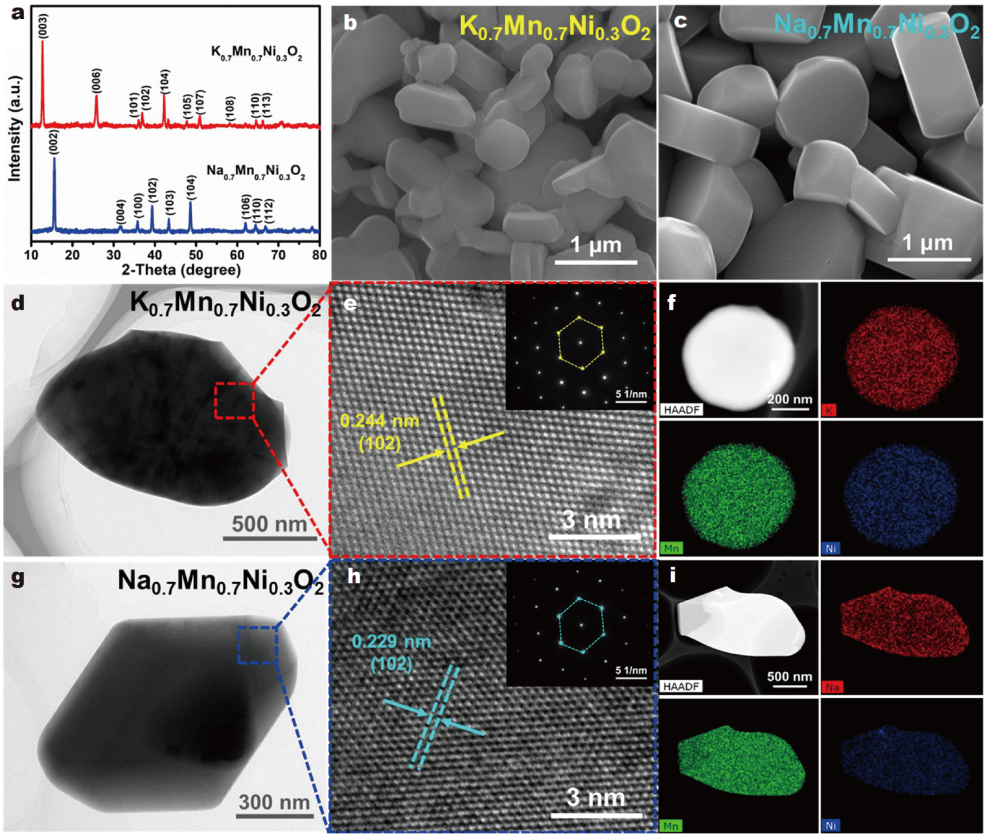

Figure 1 Structure and morphology characterizations of KMNO and NMNO. (a) XRD patterns of KMNO and NMNO. SEM images of KMNO (b) and NMNO (c). TEM image (d, g), HRTEM image (e, h), EDS mapping images (f, i) of KMNO and NMNO, respectively. Insets of (e, h) are the SAED patterns of KMNO and NMNO, respectively.

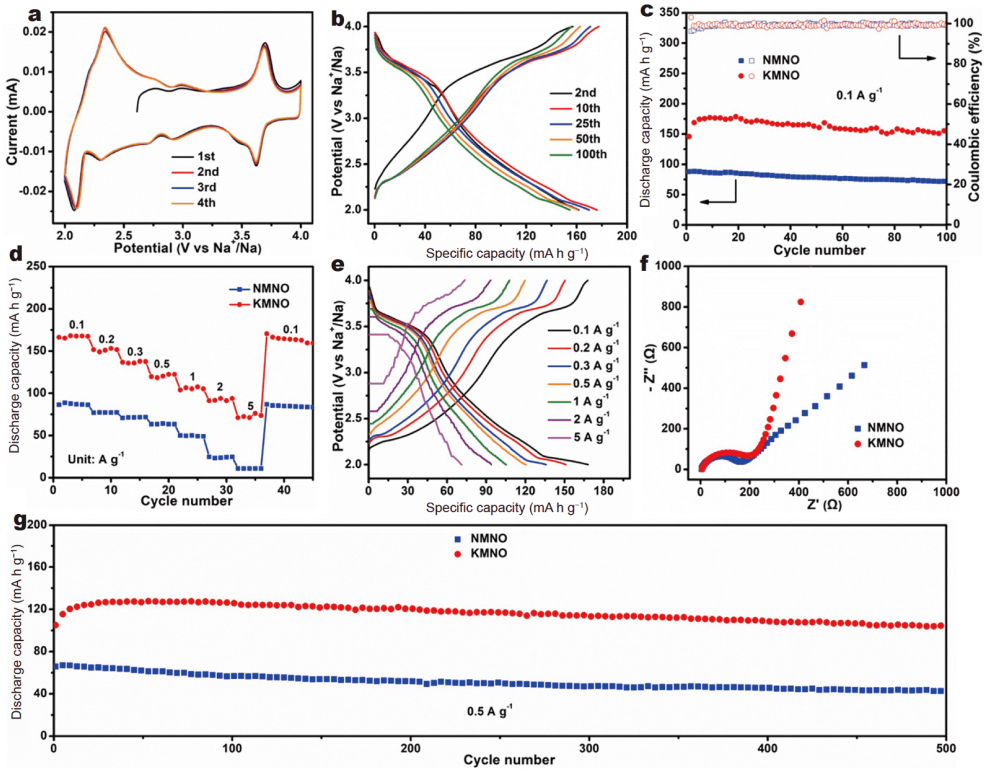

Figure 2 Electrochemical performances of KMNO and NMNO. (a) CV curves at 0.2 mV s^{-1} of KMNO during the first four cycles. (b) Charge/discharge curves of KMNO at the selected cycles at 0.1 A g^{-1}. (c) Cycling measurements for the two cathode materials tested at 0.1 A g^{-1}. (d) Rate performance of these two cathode materials at various rates ranging from 0.1 to 5 and back to 0.1 A g^{-1}. (e) Charge/discharge curves of KMNO at various rates ranging from 0.1 to 5 and back to 0.1 A g^{-1}. (f) Nyquist plots of these two cathode materials. (g) Cycling performance of KMNO tested at a high current density of 0.5 A g^{-1}.

demonstrate the complicated phase transition behavior of the Na^+ intercalation/deintercalation reaction for KMNO. In the voltage range of 2.0–4.0 V, there are five pairs of redox peaks, located at 3.58/3.69, 2.91/2.97, 2.70/2.75, 2.29/2.32, and 2.09/2.21 V. For the results of NMNO (Fig. S1a), five pairs of redox peaks situated at 3.64/3.70, 3.58/3.61, 3.30/3.34, 3.14/3.19 and 2.29/2.33 V can be observed. When tested at 0.1 A g^{-1}, the KMNO exhibits an initial discharge capacity of 161.8 mA h g^{-1} and a fabulous coulombic efficiency of 98.9% (Fig. 2b), which are higher than those of NMNO (87.8 mA h g^{-1} and 96.2%). After 100 cycles, KMNO delivers a discharge capacity of 154.7 mA h g^{-1}, which is substantially higher than that of NMNO (72 mA h g^{-1}) (Fig. 2c). Additionally, the capacity retention of KMNO reaches up to 95.6% (a slight capacity decay of 0.04% per cycle). In contrast, the NMNO only preserves 82.0% of its initial capacities. The KMNO delivers average discharge capacities of 167.6, 151.0, 135.8, 120.4, 105.3, 93.8 and 71.1 mA h g^{-1} at different current densities of 0.1, 0.2, 0.3, 0.5, 1, 2 and 5 A g^{-1}, respectively, while the discharge capacities of NMNO are 87.8, 77.3, 71.4, 64.3, 50.0, 23.7 and 11.0 mA h g^{-1} (Fig. 2d). The discharge capacity quickly recovers to 164.8 mA h g^{-1} when the current density reduced to 0.1 A g^{-1}, indicating the prominent rate performance of the KMNO. The corresponding discharge/charge curves of rate performance certify lower polarization and higher capacity reversibility of the KMNO (Fig. 2e). When tested at a high current density of 0.5 A g^{-1}, NMNO electrode suffers from drastic capacity degradation of 42.7 mA h g^{-1} and lower capacity retention of only 65% than those of KMNO (103.4 mA h g^{-1}, 82.3%) after 500 cycles (Fig. 2g). The EIS plot indicates the same charge-transfer resistance of the two electrodes based on KMNO and NMNO, while the KMNO exhibits fast diffusion resistance, mostly owing to the expanded interlayer structure (Fig. 2f). The charge-discharge curves at the selected cycles and various rates of NMNO are presented in Fig. S1b, c. Compared with some previous studies (Fig. S2 and Table S2) [43–48], KMNO as a cathode material for SIBs shows a higher energy density of 459 W h kg^{-1}, and the superior electrochemical per-

formances are ascribed to the faster diffusion coefficient due to the enlarged interlayer spacing formed by K^+ pre-intercalation.

To reveal the Na^+ intercalation/deintercalation mechanism of KMNO, *in situ* XRD patterns were first performed to investigate its structure variation before cycling (Fig. 3 and Fig. S3). When the KMNO electrode was immersed in sodium ion electrolyte for about 12 h, the interlayer (003) peak shifts dramatically from the initial 12.81° to 15.35°, with the corresponding interlayer spacing changed from 6.90 to 5.76 Å (Fig. 3a). This remarkable phenomenon is attributed to a driven ion-exchange process between potassium and sodium ions in the corresponding components, resulting in the successful transformation from $K_{0.7}Mn_{0.7}Ni_{0.3}O_2$ to $K_{0.1}Na_{0.7}Mn_{0.7}Ni_{0.3}O_2$ (Fig. S3a). The interlayer (002) peak of NMNO remains at 15.53° without shift and the interlayer spacing has no changes during the same process (Fig. 3b). The *ex situ* XRD patterns show the interlayer (003) peak changes of KMNO at the first cycle process at 0.1 A g^{-1} (Fig. 3c, d). The peak shifts from high angle (stage 2) to 12.81° (stage 3) during the first charge process from open circuit voltage to 3.75 V and slowly shifts to a low angle of 12.74° when further charged to 4 V (stage 4). The chemical composition of the electrode material changes from $K_{0.1}Na_{0.7}Mn_{0.7}Ni_{0.3}O_2$ to $K_{0.1}Mn_{0.7}Ni_{0.3}O_2$ during the first charge process. After discharging from 4 to 3.75 V (stage 5), the peak slowly moves to 12.98°, and in the subsequent conditioning process, the peak shifts to 16.07° (stage 6), which is caused by the intercalation of Na^+ ($K_{0.1}Mn_{0.7}Ni_{0.3}O_2$ to $K_{0.1}Na_{0.7}Mn_{0.7}Ni_{0.3}O_2$). Moreover, the interlayer spacing varies between 6.95 and 5.52 Å (Fig. S4), corresponding to the extraction and insertion of 0.7 Na^+ from KMNO phase in Na^+-containing electrolyte. The KMNO

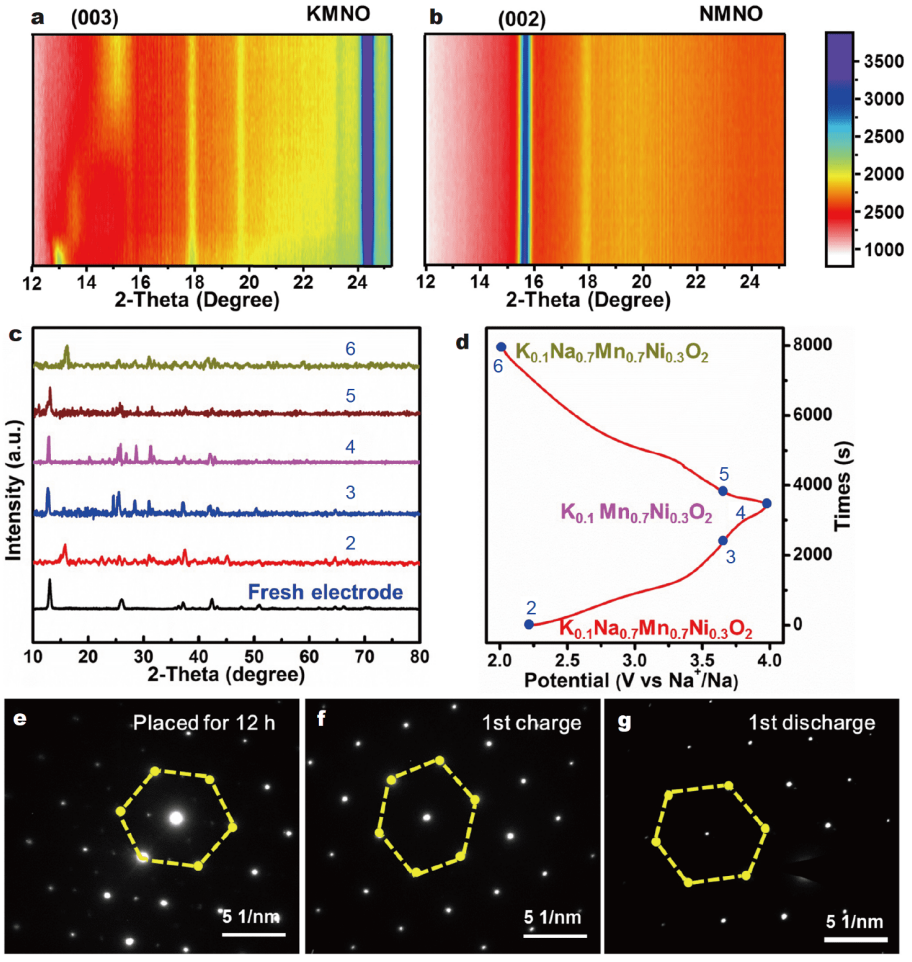

Figure 3 The sodium storage mechanism of KMNO. *In situ* XRD patterns of KMNO (a) and NMNO (b) when dropped sodium ion electrolyte and placed about 12 h. *Ex situ* XRD patterns at different stages during first cycle (c) and the corresponding voltage-time curve (d). SAED of KMNO at the stages placed for 12 h (e), 1st charge (f) and 1st discharge (g).

electrode can maintain a stable single-crystalline hexagonal structure when placed in the sodium ion electrolyte during the first two cycles, indicating the reversibility of crystal structure transformation driven by Na^+, and then the capacity retention upon sodium substitution (Fig. 3e–g and Fig. S5). After 50 cycles, XRD patterns of KMNO have almost no change from the initial state and the number of sodium ions involved in the electrochemical reaction maintains at about 0.7 (Fig. S6). The *ex situ* ICP measurements were carried out to explain the composition changes of KMNO during charge/discharge state (Table S3). To confirm no involvement of K^+ in Na^+-insertion/extraction, the first discharge, the second charge and discharge curves of KMNO cycled in fresh $NaClO_4$ electrolyte after the first charge were compared in Fig. S7. Due to self-discharge of KMNO during electrolyte exchange, the discharge capacity is lower, but the capacity and charge/discharge curve shapes during the second cycle are almost invariant.

To examine the theoretical capacity and the electrochemical kinetics of Na^+ in KMNO, the GITT was devoted to calculating the diffusion coefficient of Na^+ (D_{Na^+}) (Fig. 4a). The KMNO cathode material exhibits a theoretical discharge capacity of 185.4 mA h g^{-1}, obviously higher than that of NMNO (123.8 mA h g^{-1}) (Fig. 4b). This is because larger interlayer spacing of KMNO can provide more sodium-storing active sites. The ionic diffusion coefficient can be calculated by Fick's second laws. Due to the difference in the charging and discharging processes of KMNO and NMNO, the calculated diffusion coefficient distribution law is also different. Overall, higher values of D_{Na^+} ranging from 2.03×10^{-10} to 7.22×10^{-9} m^2 s^{-1} are obtained for KMNO (average value equals 1.61×10^{-9} m^2 s^{-1}) compared with a range of 5.19×10^{-11} to 2.64×10^{-9} m^2 s^{-1} for NMNO (average value equals 5.28×10^{-10} m^2 s^{-1}) (Fig. 4c, d). Due to the similar SEM images of the two materials after cycling (Fig. S8), the morphology has neglect effect on the difference of their capacities. The excellent electrochemical performance of KMNO is mainly due to the faster diffusion coefficient, which benefits from the larger interlayer spacing.

CONCLUSIONS

In summary, by using the pre-inserting potassium ion method, KMNO particles with more favorable interlayer spacing (6.90 Å) were exploited, resulting in a superior electrochemical performance as cathode materials for

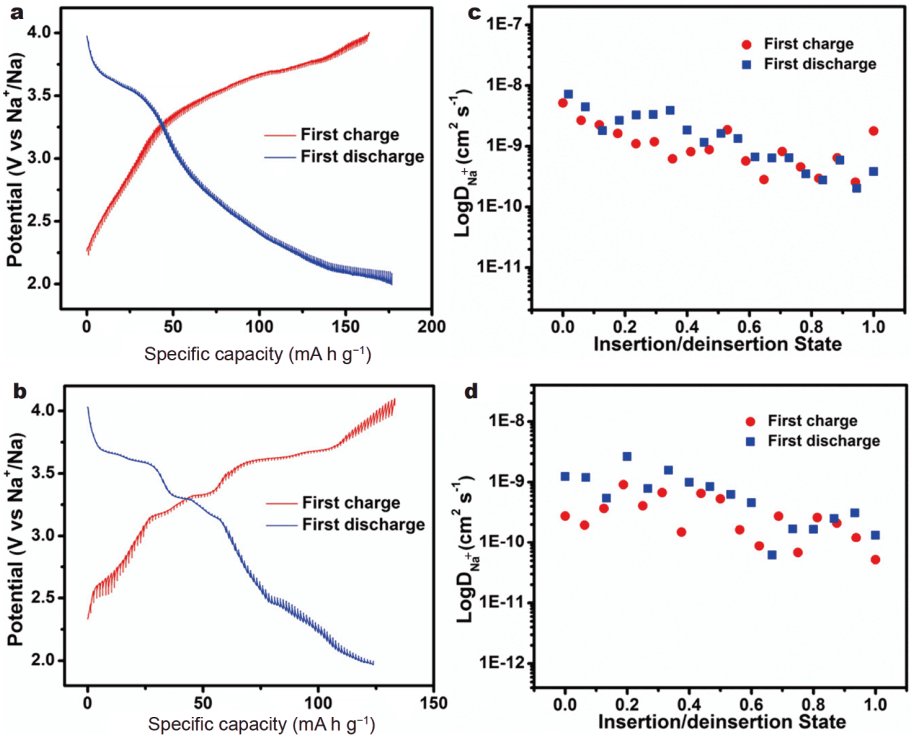

Figure 4 GITT curves and chemical diffusion coefficients of KMNO and NMNO. Potential response of KMNO (a) and NMNO (c) during GITT measurement. The calculated chemical diffusion coefficient for Na^+ in KMNO (b) and NMNO (d) *versus* specific capacity.

SIBs. The interlayer space of KMNO electrode changed from 6.90 to 5.76 Å when placed in the sodium ion electrolyte for 12 h, which was attributed to a driven ion-exchange process of potassium and sodium ions. A high reversible discharge capacity (161.8 mA h g^{-1}) and a high energy density (459 W h kg^{-1}) of KMNO are achieved at 0.1 A g^{-1}, corresponding to the reversible insertion of 0.7 Na^+. Remarkably, even cycled at a higher rate of 5 A g^{-1}, the discharge capacity is still maintained at 71.1 mA h g^{-1}. The superior electrochemical performance of KMNO is attributed to its large interlayer spacing variation (between 6.95 and 5.52 Å) and faster electrochemical kinetics (1.61×10^{-9} m^2 s^{-1}). We believe that the present work provides a strategy to design novel layered transition-metal oxide cathode materials for high energy density SIBs.

Received 5 January 2020; accepted 17 February 2020; published online 27 March 2020

1 Mai L, Yan M, Zhao Y. Track batteries degrading in real time. Nature, 2017, 546: 469–470
2 Simon P, Gogotsi Y, Dunn B. Where do batteries end and supercapacitors begin? Science, 2014, 343: 1210–1211
3 Lukatskaya MR, Dunn B, Gogotsi Y. Multidimensional materials and device architectures for future hybrid energy storage. Nat Commun, 2016, 7: 12647
4 Xiao Z, Meng J, Li Q, *et al.* Novel MOF shell-derived surface modification of Li-rich layered oxide cathode for enhanced lithium storage. Sci Bull, 2018, 63: 46–53
5 Sun YK, Chen Z, Noh HJ, *et al.* Nanostructured high-energy cathode materials for advanced lithium batteries. Nat Mater, 2012, 11: 942–947
6 Winter M, Barnett B, Xu K. Before Li ion batteries. Chem Rev, 2018, 118: 11433–11456
7 Pan H, Hu YS, Chen L. Room-temperature stationary sodium-ion batteries for large-scale electric energy storage. Energy Environ Sci, 2013, 6: 2338–2360
8 Hwang JY, Oh SM, Myung ST, *et al.* Radially aligned hierarchical columnar structure as a cathode material for high energy density sodium-ion batteries. Nat Commun, 2015, 6: 6865
9 Slater MD, Kim D, Lee E, *et al.* Sodium-ion batteries. Adv Funct Mater, 2013, 23: 947–958
10 Deng J, Luo WB, Chou SL, *et al.* Sodium-ion batteries: from academic research to practical commercialization. Adv Energy Mater, 2017, 8: 1701428
11 Yabuuchi N, Kubota K, Dahbi M, *et al.* Research development on sodium-ion batteries. Chem Rev, 2014, 114: 11636–11682
12 Kundu D, Talaie E, Duffort V, *et al.* The emerging chemistry of sodium ion batteries for electrochemical energy storage. Angew Chem Int Ed, 2015, 54: 3431–3448
13 Jia R, Shen G, Chen D. Recent progress and future prospects of sodium-ion capacitors. Sci China Mater, 2020, 63: 185–206
14 Liu FQ, Wang WP, Yin YX, *et al.* Upgrading traditional liquid electrolyte *via in situ* gelation for future lithium metal batteries. Sci Adv, 2018, 4: eaat5383
15 Wang PF, Weng M, Xiao Y, *et al.* An ordered Ni_6-ring superstructure enables a highly stable sodium oxide cathode. Adv Mater, 2019, 31: 1903483
16 Soundharrajan V, Sambandam B, Alfaruqi MH, *et al.* $Na_{2.3}Cu_{1.1}Mn_2O_{7-\delta}$ nanoflakes as enhanced cathode materials for high-energy sodium-ion batteries achieved by a rapid pyrosynthesis approach. J Mater Chem A, 2020, 8: 770–778
17 Cao A, Manthiram A. Controlled synthesis of high tap density $LiMn_{1.5}Ni_{0.5}O_4$ with tunable shapes. J Electrochem Soc, 2012, 8: 699–699
18 Sheng J, Peng C, Xu Y, *et al.* $KTi_2(PO_4)_3$ with large ion diffusion channel for high-efficiency sodium storage. Adv Energy Mater, 2017, 7: 1700247
19 Sheng J, Zang H, Tang C, *et al.* Graphene wrapped NASICON-type $Fe_2(MoO_4)_3$ nanoparticles as a ultra-high rate cathode for sodium ion batteries. Nano Energy, 2016, 24: 130–138
20 Wang PF, Yao HR, Liu XY, *et al.* Na^+/vacancy disordering promises high-rate Na-ion batteries. Sci Adv, 2018, 4: eaar6018
21 Aragón MJ, Lavela P, Ortiz G, *et al.* Nanometric P2-$Na_{2/3}Fe_{1/3}Mn_{2/3}O_2$ with controlled morphology as cathode for sodium-ion batteries. J Alloys Compd, 2017, 724: 465–473
22 Zhang Q, Huang Y, Liu Y, *et al.* F-doped O3-$NaNi_{1/3}Fe_{1/3}Mn_{1/3}O_2$ as high-performance cathode materials for sodium-ion batteries. Sci China Mater, 2017, 60: 629–636
23 Yu CY, Park JS, Jung HG, *et al.* $NaCrO_2$ cathode for high-rate sodium-ion batteries. Energy Environ Sci, 2015, 8: 2019–2026
24 Rong X, Liu J, Hu E, *et al.* Structure-induced reversible anionic redox activity in Na layered oxide cathode. Joule, 2018, 2: 125–140
25 Huang Q, Liu J, Zhang L, *et al.* Tailoring alternating heteroepitaxial nanostructures in Na-ion layered oxide cathodes *via* an *in-situ* composition modulation route. Nano Energy, 2018, 44: 336–344
26 Hwang JY, Myung ST, Choi JU, *et al.* Resolving the degradation pathways of the O3-type layered oxide cathode surface through the nano-scale aluminum oxide coating for high-energy density sodium-ion batteries. J Mater Chem A, 2018, 6: 3754
27 Qiao Y, Guo S, Zhu K, *et al.* Reversible anionic redox activity in Na_3RuO_4 cathodes: a prototype Na-rich layered oxide. Energy Environ Sci, 2018, 11: 299–305
28 Yabuuchi N, Kajiyama M, Iwatate J, *et al.* P2-type $Na_x[Fe_{1/2}Mn_{1/2}]O_2$ made from earth-abundant elements for rechargeable Na batteries. Nat Mater, 2012, 11: 512–517
29 Hou Y, Chang K, Wang Z, *et al.* Rapid microwave-assisted refluxing synthesis of hierarchical mulberry-shaped $Na_3V_2(PO_4)_2O_2F$ @C as high performance cathode for sodium & lithium-ion batteries. Sci China Mater, 2019, 62: 474–486
30 Ma C, Alvarado J, Xu J, *et al.* Exploring oxygen activity in the high energy P2-type $Na_{0.78}Ni_{0.23}Mn_{0.69}O_2$ cathode material for Na-ion batteries. J Am Chem Soc, 2017, 139: 4835–4845
31 Lee DH, Xu J, Meng YS. An advanced cathode for Na-ion batteries with high rate and excellent structural stability. Phys Chem Chem Phys, 2013, 15: 3304–3312
32 Wang PF, You Y, Yin YX, *et al.* Layered oxide cathodes for sodium-ion batteries: phase transition, air stability, and performance. Adv Energy Mater, 2017, 8: 1701912
33 Wang PF, You Y, Yin YX, *et al.* Suppressing the P2-O2 phase transition of $Na_{0.67}Mn_{0.67}Ni_{0.33}O_2$ by magnesium substitution for improved sodium-ion batteries. Angew Chem Int Ed, 2016, 55: 7445–7449
34 Wu X, Guo J, Wang D, *et al.* P2-type $Na_{0.66}Ni_{0.33-x}Zn_xMn_{0.67}O_2$ as new high-voltage cathode materials for sodium-ion batteries. J

Power Sources, 2015, 281: 18–26
35 Wang L, Sun YG, Hu LL, *et al.* Copper-substituted $Na_{0.67}Ni_{0.3-x}Cu_xMn_{0.7}O_2$ cathode materials for sodium-ion batteries with suppressed P2–O2 phase transition. J Mater Chem A, 2017, 5: 8752–8761
36 Liu Y, Fang X, Zhang A, *et al.* Layered P2-$Na_{2/3}[Ni_{1/3}Mn_{2/3}]O_2$ as high-voltage cathode for sodium-ion batteries: The capacity decay mechanism and Al_2O_3 surface modification. Nano Energy, 2016, 27: 27–34
37 Fang Y, Yu XY, Lou XWD. A practical high-energy cathode for sodium-ion batteries based on uniform P2-$Na_{0.7}CoO_2$ microspheres. Angew Chem Int Ed, 2017, 56: 5801–5805
38 Deng J, Luo WB, Lu X, *et al.* High energy density sodium-ion battery with industrially feasible and air-stable O3-type layered oxide cathode. Adv Energy Mater, 2017, 8: 1701610
39 Xie H, Wang C, Tao S, *et al.* Ball-in-ball hierarchical design of P2-type layered oxide as high performance Na-ion battery cathodes. Electrochim Acta, 2018, 265: 284–291
40 You Y, Xin S, Asl HY, *et al.* Insights into the improved high-voltage performance of Li-incorporated layered oxide cathodes for sodium-ion batteries. Chem, 2018, 4: 2124–2139
41 Zhao Y, Han C, Yang J, *et al.* Stable alkali metal ion intercalation compounds as optimized metal oxide nanowire cathodes for lithium batteries. Nano Lett, 2015, 15: 2180–2185
42 Meng J, Liu Z, Niu C, *et al.* A synergistic effect between layer surface configurations and K ions of potassium vanadate nanowires for enhanced energy storage performance. J Mater Chem A, 2016, 4: 4893–4899
43 Sathiya M, Hemalatha K, Ramesha K, *et al.* Synthesis, structure, and electrochemical properties of the layered sodium insertion cathode material: $NaNi_{1/3}Mn_{1/3}Co_{1/3}O_2$. Chem Mater, 2012, 24: 1846–1853
44 Jung YH, Christiansen AS, Johnsen RE, *et al. In situ* X-ray diffraction studies on structural changes of a P2 layered material during electrochemical desodiation/sodiation. Adv Funct Mater, 2015, 25: 3227–3237
45 Vassilaras P, Kwon DH, Dacek ST, *et al.* Electrochemical properties and structural evolution of O3-type layered sodium mixed transition metal oxides with trivalent nickel. J Mater Chem A, 2017, 5: 4596–4606
46 Oh SM, Myung ST, Yoon CS, *et al.* Advanced $Na[Ni_{0.25}Fe_{0.5}Mn_{0.25}]O_2$/C–$Fe_3O_4$ sodium-ion batteries using EMS electrolyte for energy storage. Nano Lett, 2014, 14: 1620–1626
47 Yu H, Guo S, Zhu Y, *et al.* Novel titanium-based O3-type $NaTi_{0.5}Ni_{0.5}O_2$ as a cathode material for sodium ion batteries. Chem Commun, 2014, 50: 457–459
48 Yue JL, Zhou YN, Yu X, *et al.* O3-type layered transition metal oxide $Na(NiCoFeTi)_{1/4}O_2$ as a high rate and long cycle life cathode material for sodium ion batteries. J Mater Chem A, 2015, 3: 23261–23267

Acknowledgements This work was supported by the National Natural Science Foundation of China (51872218 and 51832004), the National Key R&D Program of China (2016YFA0202603), and the Fundamental Research Funds for the Central Universities (WUT: 2017III009).

Author contributions Chen J designed and engineered the materials; Xiao Z guided the regulation in the process of material synthesis and helped complete some characterization and electrochemical performance tests; Meng J and Sheng J optimized the overall direction of the experiment; Chen J wrote the paper with support from Xu Y, Han C, Wang J and Mai L. All authors contributed to the general discussion.

Conflict of interest The authors declare no conflict of interest.

Supplementary information Supporting data are available in the online version of the paper.

Jinghui Chen received a bachelor's degree in materials science and engineering from Henan Polytechnic University in 2017. She is currently a Master candidate in materials science and engineering at Wuhan University of Technology (WUT). Her current research focuses on the synthesis and characterization of advanced materials for emerging energy storage devices.

Liqiang Mai is a Changjiang Scholar Chair Professor of materials science and engineering at WUT. He is the winner of the National Natural Science Fund for Distinguished Young Scholars and Fellow of the Royal Society of Chemistry. He received his PhD degree from WUT in 2004 and carried out his postdoctoral research with Prof. Zhong Lin Wang at Georgia Institute of Technology in 2006–2007.He worked as an advanced research scholar with Prof. Charles M. Lieber at Harvard University in 2008–2011 and Prof. Peidong Yang at the University of California, Berkeley in 2017. His current research interests focus on new nanomaterials for electrochemical energy storage and micro/nano energy devices.

具有大扩散通道的新型层状$K_{0.7}Mn_{0.7}Ni_{0.3}O_2$正极材料用于高能量密度钠离子电池

陈京辉, 肖治桐, 孟甲申, 盛进之, 徐亚楠, 王军军, 韩春华, 麦立强*

摘要 在大规模储能领域，钠离子电池作为锂离子电池的替代品，具有低成本的优势，并已被广泛研究. 由于钠离子的尺寸相对较大，大多数正极材料的扩散动力学较缓慢，循环稳定性较差，从而限制了钠离子电池的进一步应用. 本工作中，我们设计了一种新型的K^+插层式Mn/Ni基层状氧化物材料($K_{0.7}Mn_{0.7}Ni_{0.3}O_2$，表示为KMNO)，其具有稳定且扩大的扩散通道，可作为高能量密度钠离子电池的正极材料. 我们通过原位XRD和非原位ICP分析探究了KMNO电极与钠离子电解质之间自发离子交换而形成$K_{0.1}Na_{0.7}Mn_{0.7}Ni_{0.3}O_2$的过程. KMNO层间距从6.90 Å缩小到5.76 Å，大于$Na_{0.7}Mn_{0.7}Ni_{0.3}O_2$ (5.63 Å). 扩大的离子扩散通道可有效提高材料的离子扩散系数，同时材料在其框架内可提供更多的K^+储存位点. 以该KMNO为正极材料的钠离子电池具有高可逆放电容量(在0.1 A g^{-1}时为161.8 mA h g^{-1})，高能量密度(459 W h kg^{-1})，以及超高的倍率性能(在5 A g^{-1}下高达71.1 mA h g^{-1}). 本工作表明，K^+预嵌入策略使层状金属氧化物具有优异的储钠性能，为不同电池正极材料的设计提供了新的方向.

